IEEE Robotics and Automation Letters (RAL) paper presented at the
2020 IEEE/RSJ International Conference on Intelligent Robots and Systems (IROS)
October 25-29, 2020, Las Vegas, NV, USA (Virtual)

SMALLBug: A 30-mg Crawling Robot Driven by a High-Frequency Flexible SMA Microactuator

Xuan-Truc Nguyen*, Ariel A. Calderón*, Alberto Rigo, Joey Z. Ge, and Néstor O. Pérez-Arancibia

***Abstract*— We present the design, fabrication and experimental testing of SMALLBug, a 30-mg crawling microrobot that is 13 mm in length and can locomote at actuation frequencies of up to 20 Hz. The robot is driven by an electrically-powered 6-mg bending actuator that is composed of a thin *shape-memory alloy* (SMA) wire and a carbon-fiber piece that acts as a loading leaf-spring. This configuration enables the generation of high-speed thermally-induced phase transformations of the SMA material to produce high-frequency periodic actuation. During development, several actuator prototypes with different mechanical stiffnesses were tested and characterized by measuring their bending motions when excited with *pulse-width modulation* (PWM) voltages with a variety of frequencies and *duty cycles* (DCs). In a similar manner, the displacement–force characteristic of the actuator chosen to drive SMALLBug was identified by measuring its bending displacements under a number of different loads ranging from 4.22 to 83.8 mN. The locomotion capabilities of SMALLBug were experimentally tested at three different input actuation frequencies, which were observed to produce three distinct gaits. At the *low* frequency of 2 Hz, the robot locomotes with a *crawling gait* similar to that of inchworms; at the *moderate* frequency of 10 Hz, the robot advances smoothly at an approximately constant speed using a *shuffling gait*; and at the *high* frequency of 20 Hz, the robot generates small and fast jumps in a *galloping gait*, reaching average speeds of up to 17 mm $\cdot$ s^{-1}, equivalent to 1.3 *body-lengths per second* (BLPS).**

I. INTRODUCTION

The development of mobile microrobots is driven by the vision of creating swarms of fully autonomous mm-to-cm-scale agents that can travel and operate within constrained spaces that are inaccessible to humans and human-scale robots. In order for a microrobot to perform useful tasks independently, it must be able to generate large forces relative to its size and weight; therefore, new mm-scale microactuators with *high work densities* (HWDs) must be developed to advance the autonomy of micro-agents. To this end, we introduce a novel microactuator with a weight of 6 mg, a length of 12 mm and a volume of 1.89 mm^3, which exploits the HWDs of *shape-memory alloy* (SMA) wires and can achieve high operation frequencies (up to 20 Hz). To demonstrate the functionality and performance of the actuator, a series of stand-alone characterization experiments were performed, including the measurement of the output displacements excited by *pulse-width modulation* (PWM) voltages with a variety of frequencies and *duty cycles* (DCs). We further studied the capabilities of the microactuator by developing and experimentally testing a 30-mg crawling robot that we refer to as *SMA little locomoting* (SMALL) *bug*, or SMALLBug for short, shown in Fig. 1. This prototype has a length of 13 mm and can locomote at actuation frequencies of up to 20 Hz, achieving average speeds as high as 17 mm $\cdot$ s^{-1}, which is equivalent to 1.3 *body-lengths per second* (BLPS).

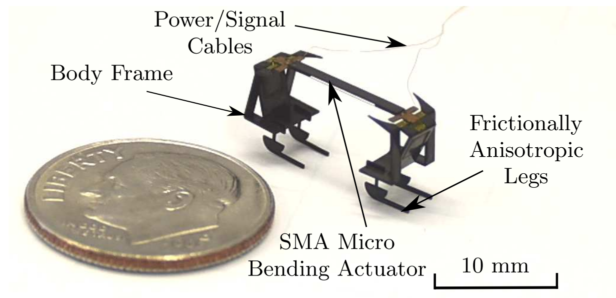

Fig. 1. **Photograph of SMALLBug.** An SMA bending microactuator connects the two halves of the 2-Σ body frame. Frictionally anisotropic legs enable forward motion when the actuator bends cyclically. A U.S. dime is included for scale.

The most common actuation methods used in microrobotics are based on piezoelectricity [1]–[3], electromagnetics [4]–[9] and SMAs [10]–[13]. The first two technologies are often preferred due to their wide actuation bandwidth, which enables high-frequency operation. Recent research based on these methods has produced a wide variety of microrobotic crawlers, some of which are compared to SMALLBug in the velocity–mass chart in Fig. 2. The magnetically-actuated crawlers reported in [6]–[9] are relatively fast and light; however, the difficulty of their operation outside laboratory conditions impairs their versatility. SMA-based actuators exhibit advantages and disadvantages with respect to other technologies. The most important advantage is that the work densities associated with SMA wires are significantly higher than those of any other known actuation methods [14], [15]. The main disadvantage is the difficulty to achieve high speeds of operation because these are limited by the cooling times of SMA materials during cyclic phase transformations. Another limitation is that the maximum attainable contractions of SMA wires do not exceed 5 %, even under perfect laboratory conditions.

The behavior of an SMA wire is determined by the *shape-memory effect* (SME) and the *superelasticity* property [14], according to which SMA materials can exist in two distinct crystal phases, *martensite* or *austenite*, depending on their temperature and stress conditions. Thermally-induced transitions between crystal states are the mechanism responsible for macroscale geometric deformations of an SMA material. Specifically, at temperatures lower than the *reverse* transition point, an SMA material exists in a martensite

This work was supported in part by the *National Science Foundation* (NSF) through NRI Award 1528110, in part by the *Defense Advanced Research Projects Agency* (DARPA) through Contract HR0011-19-C-0048, and in part by the USC Viterbi School of Engineering through a start-up fund to N. O. Pérez-Arancibia.

*These authors contributed equally to this work.

The authors are with the Department of Aerospace and Mechanical Engineering, University of Southern California (USC), Los Angeles, CA 90089-1453, USA (e-mail: xuantrun@usc.edu; aacalder@usc.edu; rigo@usc.edu; zaoyuang@usc.edu; perezara@usc.edu).

state, corresponding to a monoclinic crystal molecular configuration; while at temperatures higher than the *forward* transition point, an SMA material exists in an austenite state, corresponding to a cubic crystal molecular configuration [16]. Consistently, an SMA wire remains *contracted* in the austenite state and *extended* in the martensite state; thus, *Joule* heating can be used to thermally excite an SMA wire to induce contraction while extension can be achieved through passive cooling. Experiments demonstrating this excitation approach are reported in [17].

Recent research has shown considerable progress toward overcoming the limitations of SMA-based actuation. For example, [18] and [19] report a 56-mm-long SMA actuator, composed of thin NiTi wires with a diameter of 150 µm and a central 3D printed structural piece, that can achieve actuation frequencies in the order of 10 to 35 Hz and output displacements in the order of 120 µm. However, fabrication issues prevent this design from being scaled down below 20 mm. To a certain extent, the flexible bending actuator presented in this letter is the result of applying novel design and fabrication methods to realize the ideas in [18] and [19] at the mm-scale. In particular, despite its small volume and weight, the actuator developed to drive the SMALLBug prototype in Fig. 1 can generate oscillatory output displacements in excess of 300 µm at 20 Hz. Three elements contributed to this breakthrough in SMA actuation technology.

The first element is a design based on the use of extremely thin NiTi (∼56 % Nickel; ∼44 % Titanium) SMA wires with a diameter of only 38.1 µm, which define a very small total volume and a comparatively large total surface area. Thus, recalling that the rates of heat dissipation due to conduction and convection are proportional to the total surface area of a cooling body and that the thermal energy contained in a body is proportional to its volume, by using thin SMA wires excited through *Joule* heating, we are able to force a fast transition of the SMA material from martensite to austenite due to the small thermal mass and, also, from austenite to martensite due to the relatively large surface area of the system. The second element is the use of a central piece of *carbon fiber* (CF) that functions as a leaf-spring that applies the loading stress that the SMA material requires to exploit the SME. The third element is the utilization of the *smart composite microstructures* (SCM) method [20] to miniaturize the designs to the mm-scale. For the purposes of robotic design, in addition to basic characterization experiments, we tested and compared actuators with different thicknesses and, therefore, stiffnesses. Furthermore, the displacement–force characteristic of the actuator that drives SMALLBug was identified by measuring its bending displacements under a number of different loads ranging from 4.22 to 83.8 mN.

In the rest of the paper, Section II describes the design and fabrication of the microrobotic components and the final assembly of SMALLBug; Section III presents the experimental characterization of several microactuator prototypes; Section IV shows locomotion experiments that demonstrate the capabilities of SMALLBug; lastly, Section V states some conclusions.

II. DESIGN AND FABRICATION

As depicted in Fig. 3(a), a SMALLBug prototype consists of three main components: an SMA-based bending actuator, a body frame composed of two Σ-shaped halves, and four legs capable of generating anisotropic friction. The actuator is composed of a flat flexible structural CF beam that functions as a leaf-spring; two structural ends coated with copper (Cu), designed to facilitate electrical connections and mechanical assembly; and a looped NiTi SMA wire that is threaded through two orifices at one extreme of the structural beam, then threaded through the orifices at the other extreme, knotted at its ends, and fixed using *cyanoacrylate* (CA) glue while in a martensitic state (extended). In this configuration, the CF leaf-spring bends when the SMA wire is thermally excited and, as a consequence, shortens as the SMA material reaches an austenitic state. Thus, by repeatedly *Joule* heating and passively cooling the SMA wire, the actuator bends cyclically, and this motion is directly transmitted to the 2-Σ body frame to periodically change the angles of contact between the legs and the ground, as depicted in Fig. 3(b). This interaction produces forward motion each time a bending-and-straightening cycle is completed. The locomotion mode and speed of SMALLBug depend on the frequency and instantaneous displacement output of the SMA actuator and, also, the contact surface between the legs and the ground. Through iterative design of the shaped of the legs, we can program the robot to travel in the desired forward direction. The fabrication of the robot is based on the SCM method [20], according to which a monolithic stack composed of layers of different materials is built to create 2D structures with laser-machined assembly features such as hinges and slots. These 2D structures are then folded and glued to create the 3D functional parts that compose a microrobot.

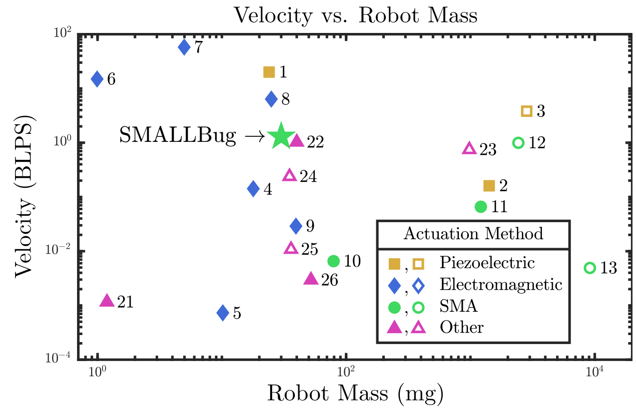

Fig. 2. **Speeds of a number of state-of-the-art crawling microrobots.** Hollow markers indicate autonomous robots, while filled markers indicate non-autonomous robots. SMALLBug is represented by the green star. The data points were compiled using information from [1]–[13], [21]–[26].

A. *Actuator*

The two Cu-coated ends of the actuator serve two essential purposes: structural connection of the actuator with the 2-Σ frame and electrical connection of the SMA wire with the external power source, as shown in Fig. 3(a). From both the mechanical and electrical perspectives, the looped wire is attached to the bending beam in a way such that it functions as two parallel wires. Accordingly, when a voltage is applied across the looped SMA wire via the Cu-coated ends, two identical electric currents pass through the two branches of the wire, thus heating the SMA material to induce the contraction of two fibers that work mechanically

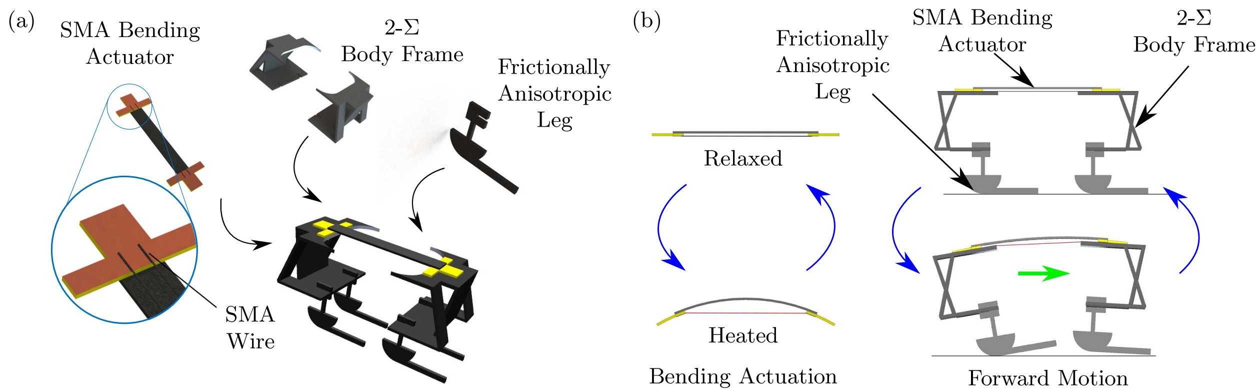

Fig. 3. **Robotic design. (a)** SMALLBug consists of three elements: a high-frequency bending SMA actuator, a 2-Σ body frame, and frictionally anisotropic legs. **(b)** Forward motion generation. The geometry of the legs allows smooth rotation in the counterclockwise direction while hindering rotation in the clockwise direction as the feet act as physical stops. Upon actuator activation, the interaction of the legs with the ground produces forward motion.

in parallel. Since the two extremes of the central CF beam are rigidly fixed to the Cu-coated structural ends, a contraction of the looped SMA wire pulls the actuator ends toward each other, forcing the CF beam to bend as depicted in Fig. 3(b). This bending displacement can be utilized to generate an anisotropic-friction-based cyclic anchor-and-slide pattern to produce unidirectional locomotion in a similar fashion as in the experiments shown in [27], [28]. In the designed robotic configuration (see Fig. 3(b)), by fixing the looped SMA wire to the extremes of the structural beam, the distance between the two Cu ends is coupled to the length of the two parallel branches of the looped wire. Since the central CF beam functions as a leaf-spring, it stores elastic energy when bent; consistently, the actuator recovers its original flat shape when the exciting voltage is turned off. Periodic actuation is generated by simply repeating the bending-and-straightening cycle.

To achieve high-frequency SMA-based microactuation, we introduce two design innovations that directly address the two major issues associated with SMA materials. First, to increase the cooling rate of the SMA material compared to other reported SMA-based actuators, we employ an SMA wire with the very small diameter of 38.1 µm. The small thermal mass and relatively large surface area of this wire allow the SMA material to be heated up and cooled down at high rates during operation; namely, in the order of 1200 and 130 $\mathrm{K \cdot s^{-1}}$, respectively. This feature is relevant because the velocity of transition from a martensite state to an austenite state, and vice versa, is also high. The main drawback of using a single thin SMA filament is the small amount of force that can be generated; therefore, we use a looped SMA wire that functions as two filaments in parallel. Thus, the SMA material still cools down quickly, but the force generated is twice as much as that produced by a single filament, and large enough (up to 380 mN) to bend the central CF beam of the actuator and drive a 30-mg SMALLBug prototype. The second design innovation is the integration of the central CF leaf-spring that provides structural support and maintains the two branches of the looped SMA wire in tension. These innovations enabled us to iteratively realize the design of the mechanically-robust flexible bending 6-mg actuator that drives SMALLBug at frequencies as high as 20 Hz with output displacements in excess of 300 µm. Note that the extremely low weight of the device reflects the fact that its envelope is 12 mm×3 mm×0.25 mm and its total volume is only 1.89 $\mathrm{mm^3}$.

The four-step process employed to fabricate the actuator is depicted in Fig. 4(a). In Step 1, a piece of Cu-coated fiberglass-epoxy laminated material (CuFR4) is laser-cut to create a jig. We use a diode-pumped solid-state ultraviolet laser (Photonics Industries DCH-355-3) with a wavelength of 355 nm and a spot diameter of 10 µm. The jig is perforated with orifices through which the SMA wire is threaded (see the inset of Step 2 in Fig. 4). The Cu-coated side of the CuFR4 material provides a surface to which electrical connections are made in order to heat the SMA wire. In Step 2, after the jig is cut, the SMA wire is looped through the holes in the CuFR4 and tied using a simple knot to maintain tension. To secure the attachment, a small amount of CA glue is applied at the knot, which prevents unraveling and holds the wire in place on the CuFR4 jig. In Step 3, a flat piece of CF, which will become the leaf-spring, is glued onto the Cu-coated ends of the jig. By design, the stiffness of an actuator is primarily determined by the thickness of the central CF beam. Consistently, to obtain CF beams with different stiffnesses, we fabricate laminates with different numbers and orientations of unidirectional Tenax CF prepreg layers, where 0° indicates an alignment with the length of the actuator. Namely, we use 0-90-90-0 to obtain a thickness of 90 µm; 0-90-90-0-0-90-90-0 to obtain 180 µm; and 0-90-0-0-90-0-0-90-0 to obtain 230 µm. Lastly, in Step 4, a release cut is performed to separate the actuator from the jig before being installed in a SMALLBug prototype.

B. Two-Sigma (2-Σ) Body Frame

The 2-Σ body frame consists of two halves, each made from a multi-material stack composed of two layers of CF and an intermediate layer of polyimide film (Kapton). The purpose of the Kapton layer is to add features that enable folding and reconfiguration, according to the SCM method [20], from a 2D shape to the 3D sigma structure that characterizes each half of the body frame as depicted in Fig. 3. This geometrical Σ shape enables the transformation of the bending displacements produced by the actuator into variations of the angle of contact of the robot's legs with the ground. The three-step process employed to fabricate each half of the 2-Σ frame is illustrated in Fig. 4(b). In Step 1,

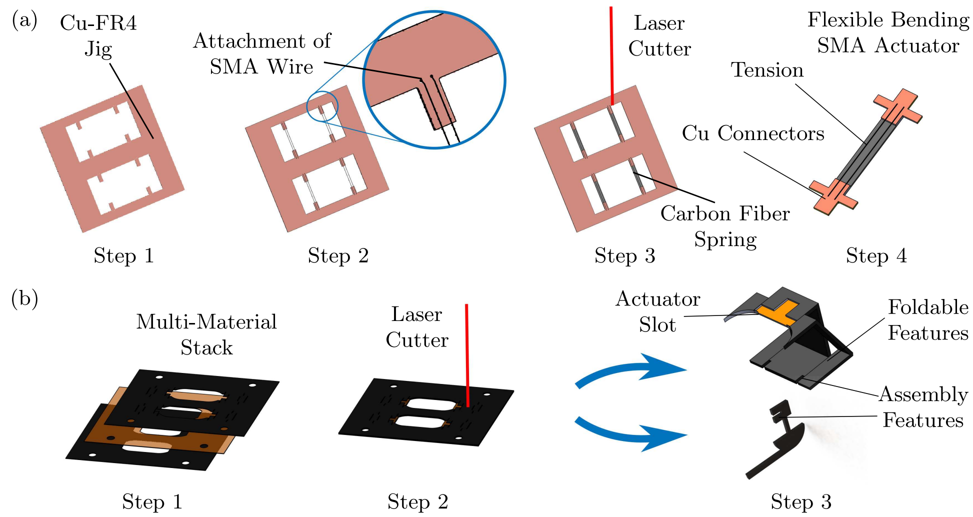

Fig. 4. **Fabrication of SMALLBug components. (a) Fabrication of SMA-based bending actuators.** The process consists of four steps. In Step 1, a layer of CuFR4 is cut into the desired shape, with orifices that help position the SMA wires. In Step 2, SMA wires are threaded through the orifices in the CuFR4 layer, then held in place by simple knots and permanently fixed with glue. In Step 3, CF beams are glued onto the back of the jig to maintain the SMA wires in tension. Finally, in Step 4, the jig is laser-cut to release the actuators. Electrical connections are then made by attaching wires to the Cu terminals using conductive epoxy. **(b) Fabrication of the 2-Σ body frame and frictionally anisotropic legs.** In Step 1, a stack is made from two layers of CF and an intermediate layer of polyimide Kapton film. A sheet adhesive (Dupont Pyralux) is used to bond the layers. This stack is cured at high temperature and pressure using an automatic hydraulic press. The CF pieces contain pre-cut features that facilitate folding. In Step 2, the corresponding stacks are release-cut to obtain the Σ-shaped body frame pieces and legs. Finally, in Step 3, the two halves of the 2-Σ body frame are folded from 2D shapes to 3D structures. The legs, once released, are ready to be installed on the body using interlocking features.

layers of pre-cut CF, Kapton and adhesive are prepared and aligned, then cured into a single stack. In Step 2, integrated features, such as flexure mechanisms that facilitate folding, are cut, and then each final 2D piece is released. Finally, in Step 3, the released precursory 2D pieces are folded and structurally reinforced with CA glue to obtain the 3D parts with the characteristic Σ shape.

C. Frictionally Anisotropic Legs

Cyclic friction-based robotic locomotion has been studied and successfully realized in the research presented in [27]–[29] and references therein. As shown in Fig. 3, SMALLBug has two front and two rear legs capable of generating anisotropic friction. As depicted in Fig. 3(b), the legs have feet with a 3D geometry such that when rotated counterclockwise, the friction with the ground is *low* due to the rounded surface of contact; in contrast, when rotated clockwise, the friction with the ground is *high* due to the edged surface of contact. Accordingly, when the actuator bends, the front legs tend to *anchor* to the ground and the back legs *slide* forward; and, when the actuator straightens, the front legs *slide* forward and the back legs tend to *anchor* to the ground. Consistently, cyclic bending actuation causes SMALLBug to locomote forward (toward the right in Fig. 3(b)). During fabrication, the legs are laser-cut, ready to be assembled, from the same multi-material stack from which the 2-Σ body frame is cut. Further details are illustrated in Fig. 4(b).

D. Final Assembly

The final construction of SMALLBug relies on the use of assembly features such as slots and matching connecting joints that are reinforced with CA glue. The actuator is installed onto the 2-Σ body frame using cross-shaped alignment features. The legs are attached to the body frame through interlocking slots and fixed with CA glue. Two 49-AWG Cu wires are installed, one on each Cu-coated end of the actuator, to apply the voltage that simultaneously powers the robot and serves as the control signal. For the experiments in Section IV, the length of the wires was chosen to be sufficiently long so that the robot can travel a significant distance (∼10 cm) without noticeably tensioning them; consistently, the wire diameter was chosen to be just large enough to reliably withstand the electrical current used to *Joule* heat the SMA material. The electrical connections between the wires and actuator Cu-ends are made using conductive epoxy (MG Chemicals extreme conductivity silver epoxy adhesive).

III. ACTUATOR CHARACTERIZATION

During characterization, the tested actuator is driven using a PWM voltage signal with specified parameters (frequency, *on*-height and DC). A Simulink Real-Time setup is used to generate the exciting PWM signal, which is then sent to an externally-powered MOSFET required to stabilize the exciting voltage and provide the currents needed to *Joule* heat the SMA material. The *instantaneous output displacement* (IOD) of the actuator at its distal end is measured using a laser sensor (Keyence LK-031) at a sampling rate of 1 kHz. The signals corresponding to two cycles of operation of a 90-μm-thick actuator are shown in Fig. 5. Here, the exciting PWM signal is shown in *red* and the measured IOD is shown in *blue*. During a PWM period, the voltage applied across the Cu-coated ends of the actuator is either *on* or *off*; in this case, *on* corresponds to 10 V and *off* to 0 V. The span of time over which the exciting voltage is *on* is determined by the DC, which here we express as a percentage of the signal period. For example, in Fig. 5, the PWM period is 1 s and the DC is 5 %, which implies that, during an actuation cycle, for 50 ms a current is passed through the looped SMA wire to induce *Joule* heating. In the case of the actuator that drives SMALLBug, wide DCs cannot be used because the thin Cu wires used for electrical connection might overheat. In fact, we have experimentally observed that the Cu wires break due

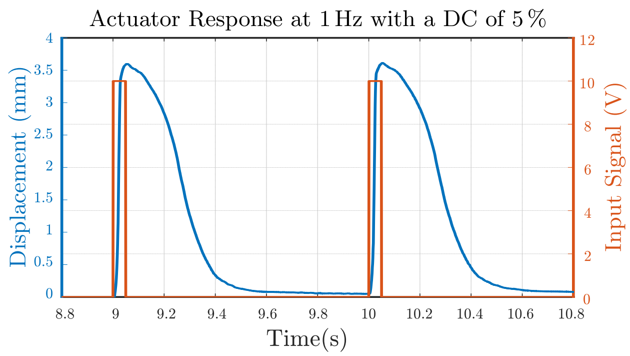

Fig. 5. **Measured instantaneous output displacement of a 90-μm-thick actuator and exciting PWM signal.** In this case, the PWM input has a frequency of 1 Hz, an *on*-height of 10 V and a DC of 5 %. As the instantaneous measurements show, the SMA wire contracts during the *on* portion of the PWM signal as it heats up and its crystal structure changes from martensite to austenite. For the remainder of the period, the current through the wire is maintained at zero to allow cooling, which corresponds to extension of the wire.

to high currents (>300 mA) well before the SMA material becomes noticeably damaged, thus acting as protective fuses. Consistently, the diameter of the Cu wires is the limiting factor when choosing the DC of excitation.

In the analysis of the characterization experiments, we consider the *steady-state* actuator response and define the *measured actuation displacement output* (MADO) as the difference between the maximum and minimum values of the measured IOD during an actuation cycle. For example, in Fig. 5, the average MADO of the two plotted cycles is 3.67 mm. Experimental evidence indicates that to maximize the average of the steady-state MADO of an actuator, different DCs are required for different frequencies of actuation. This phenomenon is demonstrated through Fig. 6, which shows the measured IODs generated by a 90-μm-thick actuator excited with a PWM signal with an *on*-height of 10 V at frequencies of 5, 10, 15 and 20 Hz. In this case, the maximum average of the steady-state MADO is achieved with a DC of 7.5 % at 5 Hz, but with a DC of 10 % at 10, 15 and 20 Hz. These plots also clearly show that the MADO decreases as the frequency increases. This pattern indicates that at higher frequencies, as the time available for the SMA material to heat up and cool down decreases due to the shortened period of the PWM signal, the actuator has less time to bend and straighten. Also, dynamic phenomena such as the added-mass effect become more relevant at higher frequencies, which might increase the amount of force required to bend the leaf-spring and, as a consequence, might decrease the bending of the actuator. Fig. 7(a) shows three photographic composites of the steady-state minimum and maximum bending displacements during one PWM cycle of a 90-μm-thick actuator operating at 1, 5 and 10 Hz with DCs of 5, 7.5 and 10 %, respectively. These cases correspond to the same experiments that produced the data in Figs. 5, 6(a) and 6(b).

Another relevant phenomenon observable in Figs. 5 and 6 is the steady-state bias produced by a temperature drift of the SMA material. Clearly, in the case shown in Fig. 5, the steady-state bias is almost negligible and displacement drift is not observed. However, in Fig. 6(a), the drift becomes noticeable and in Figs. 6(b)–(d), it becomes one of the most salient features of the signals. From these plots we deduce that as the PWM frequency is increased, the SMA material has less time to cool down sufficiently to reach a fully martensitic state during a PWM cycle. Therefore, the SMA wire remains partially contracted and the actuator partially bent when the next cycle begins. During the transient period (first 2 to 3 s), the temperature does not return to its original value at the start of the cycle. In this way, the initial condition for the next actuation cycle increases and temperature drift is produced; the steady state is reached when the periodic initial condition becomes constant. For overly wide DCs, runaway instabilities cause the Cu wires to burn. In the cases in Fig. 6, the displacement drift increases for 2 to 3 s, after which the bias reaches a steady-state value as the SMA wire begins to operate according to a minor hysteretic loop. For PWM frequencies of 10 Hz or higher, the steady-state bias produced by temperature drift is approximately equal to or larger than 2 mm, and larger than 0.5 mm for a frequency of 5 Hz. Note that in the computation of the MADO, the steady-state bias produced by drift is discounted for comparison purposes.

To study the relationship between stiffness and actuator response, we fabricated three actuators with CF beams of different thicknesses. The selected values are those that were discussed in Section II-A, i.e., 90, 180 and 230 μm, which span a range in which the beams are flexible enough to bend and strong enough to withstand cyclical loading. Using lamination theory [30], we estimate that the longitudinal bending stiffnesses of the respective beams are 10.04, 55.86 and 92.65 $\mu\mathrm{N}\cdot\mathrm{m}$. During the tests, the three actuators were excited using PWM signals with the same *on*-height of 10 V and a variety of frequencies; namely, those in the set $S_\mathrm{f} = \{1, 2.5, 5, 7.5, 10, 12.5, 15, 17.5, 20\}$ Hz. The DCs were selected to maximize the average of the steady-state MADO for each frequency in S_f. The results for the three different actuators are shown in Fig. 7(b). Here, the averages of the MADOs obtained with the optimal DCs, calculated using 10 steady-state actuation cycles, are plotted as functions of the PWM frequency. The vertical bars indicate the corresponding *experimental standard deviations* (ESDs). This plot consistently shows that, regardless of the stiffness, the MADO decreases as the frequency increases. This pattern entirely agrees with the results in Fig. 6. For all the tested frequencies, the maximum-average MADOs generated by the 90-μm-thick actuator are significantly better than those produced by the other two devices. This result agrees with the notion that the least stiff actuator, which corresponds to the thinnest CF beam, requires smaller forces to bend; accordingly, as the thickness, and therefore the stiffness, is increased, the resulting displacement is decreased.

To empirically find the DC that maximizes the average of the steady-state MADO for a fixed PWM frequency and the constant *on*-height of 10 V, we performed a series of experiments in which the DC is varied while the other PWM signal parameters are maintained constant. For example, Fig. 7(c) shows the averages of the MADOs, calculated using 10 steady-state actuation cycles, of the 90-μm-thick actuator as a function of the DC for values in the set $S_\mathrm{DC} = \{1, 2, 4, 6, 7.8, 8, 10, 12, 14, 16, 18, 20\}$ % for a frequency of 1 Hz. The vertical bars indicate the corresponding ESDs. Clearly, the DC that maximizes the average of the steady-state MADO lies between 7 and 9 %; in fact, we estimate that the optimal DC is 7.8 %. We observed

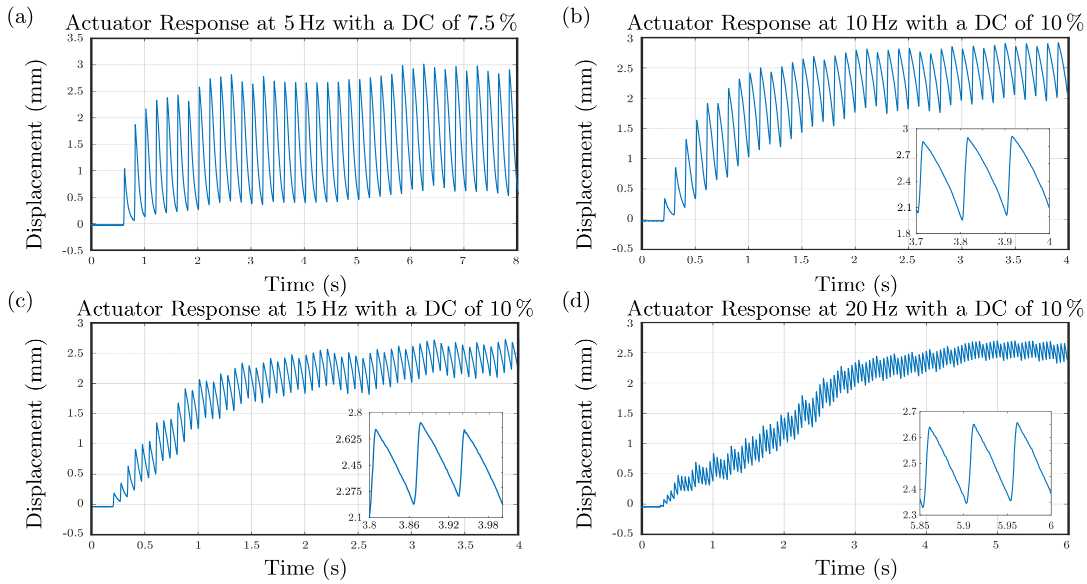

Fig. 6. **Measured IODs during the characterization of the 90-µm-thick actuator.** **(a)** Displacement for a DC of 7.5 % at 5 Hz. With these parameters, some displacement drift is observed, which indicates that the SMA wire does not have sufficient time to completely cool down and return to its original length. The average steady-state MADO, based on the last 10 cycles, is 2.43 mm. **(b)** Displacement for a DC of 10 % at 10 Hz. With these parameters, the actuator response reaches steady state after drifting almost 2 mm. The average steady-state MADO, based on the last 10 cycles, is 0.83 mm. **(c)** Displacement for a DC of 10 % at 15 Hz. With these parameters, the actuator response reaches steady state after drifting more than 2 mm. The average (last 10 cycles) steady-state MADO is 0.52 mm. **(d)** Displacement for a DC of 10 % at 20 Hz. With these parameters, the actuator response reaches steady state after drifting more than 2.3 mm. The average steady-state MADO, based on the last 10 cycles, is 0.32 mm. Despite the significant drift, the steady-state MADO is more than adequate to drive a SMALLBug prototype.

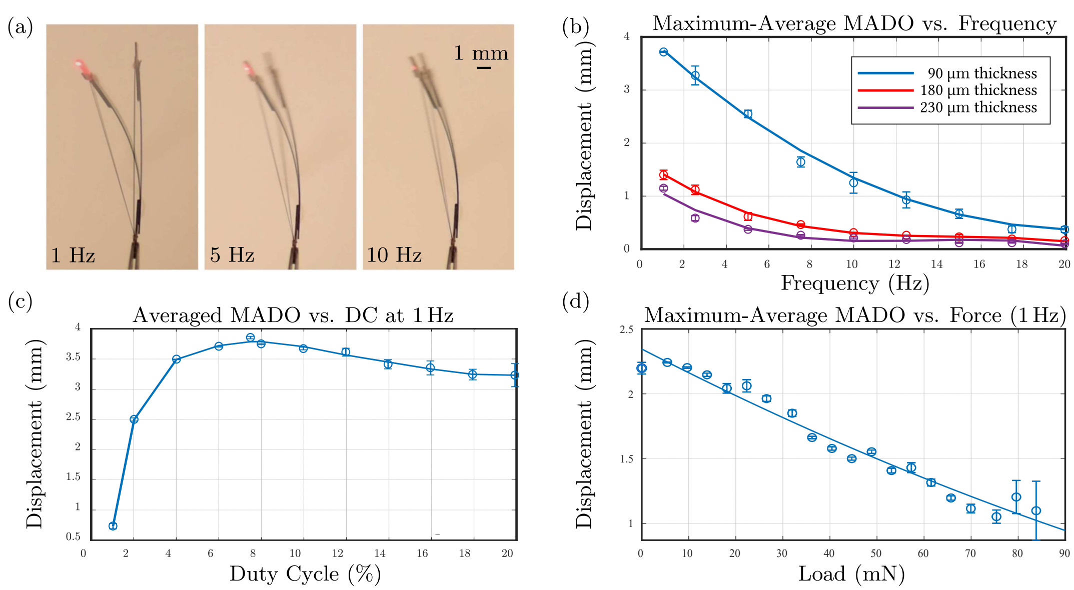

Fig. 7. **Actuator characterization.** **(a)** Photographic composites of the steady-state minimum and maximum bending displacements during one PWM cycle of the 90-µm-thick actuator operating at 1, 5 and 10 Hz with DCs of 5, 7.5 and 10 %, respectively. The complete experiments can be seen in the accompanying supplementary movie. **(b)** Experimental displacement–frequency plots for three actuators with different thicknesses. In each experiment, the exciting input is a PWM signal with an *on*-height of 10 V, and for each frequency, we selected the DC that maximizes the average of the steady-state MADO. The largest MADOs were obtained with the 90-µm-thick actuator. Each point represents the average of 10 steady-state values and the vertical bars indicate the ESDs. **(c)** DC sweep. To find the DC that maximizes the average of the steady-state MADO of the 90-µm-thick actuator at 1 Hz, we perform a series of tests by exciting the device with the fixed PWM frequency of 1 Hz and constant *on*-height of 10 V, while the DC is varied. In this case, the optimal DC is 7.8 %. Each point represents the average of 10 steady-state values and the vertical bars indicate the ESDs. **(d)** Maximum-average steady-state MADOs of a 90-µm-thick actuator operating at 1 Hz under different loads. As the load increases, the ability of the actuator to deflect diminishes. Each point represents the average of 10 steady-state values and the vertical bars indicate the ESDs. In the supplementary movie, we show the experiment corresponding to a load of 83.8 mN.

a similar trend for each of the tested frequencies; starting from 1 %, as the DC is increased, the displacement rapidly increases to reach a peak, then smoothly decreases. This pattern reflects a trade-off between the heating and cooling times as for DCs wider than the experimentally-optimal heating time of the SMA material, the wire stops contracting while its temperature continues to increase. Also, the *off*-time of the PWM cycle is reduced and the SMA material has less time at its disposal to cool down; as a result, the actuator might not have enough time to return to the initial

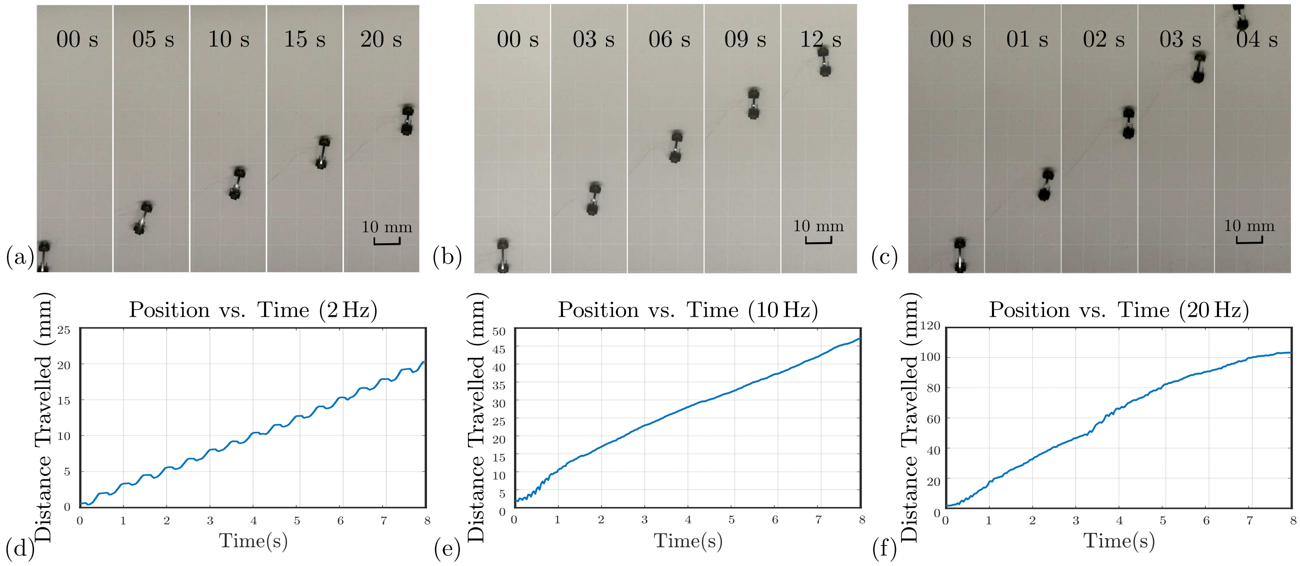

Fig. 8. **Photographic sequences and position–time plots of locomotion experiments. (a)–(c)** Top views of SMALLBug locomoting with actuation frequencies of 2, 10 and 20 Hz. At 2 Hz, the robot generates a *crawling* gait, and its position–time plot in **(d)** exhibits a characteristic stepping pattern. At 10 Hz, the robot generates a *shuffling* gait, and its position–time plot in **(e)** shows an approximately constant velocity, characteristic of this type of motion. At 20 Hz, the robot generates a *galloping* gait with the position–time relationship shown in **(f)**. This plot exhibits sudden slope changes, which indicates that the velocity of the robot changes unpredictably during the test. At this frequency, the maximum average speed obtained was $17\,\mathrm{mm}\cdot\mathrm{s}^{-1}$ (1.3 BLPS).

position of the cycle before the next actuation period starts. In contrast, the opposite happens when the DC is narrower than the experimentally-optimal heating time because the SMA material does not have enough time to reach a fully austenitic state, resulting in incomplete bending and a small MADO.

Lastly, we performed tests on the 90-µm-thick actuator under loading. During the tests, the actuator was positioned horizontally with the carbon fiber side downward and the SMA side upward, with only the tip extending off of the experimental table. We loaded the actuator by hanging several different weights off the tip and measured the IODs produced by the actuator while operating at 1 Hz. The *on*-height was maintained at 10 V and the DCs were varied within the range of 5 % to 40 %, depending on the load, to empirically maximize the 10-cycle average of the steady-state MADOs. The results are shown in Fig. 7(d) where the vertical bars correspond to the ESDs; as expected, the actuator deflected the most with low loads and its maximum-average steady-state MADOs decreased as the load was increased. Even with the highest load tested of 8.545 g (285 times the weight of SMALLBug), the actuator was able to lift the weight a distance of over 1 mm (see the accompanying supplementary movie). These results demonstrate the high work density of the actuator and its potential to withstand heavy loading. We estimate from the voltage signals and measured electrical resistance that the average power consumption of the 90-µm-thick actuator is in the order of 100 to 200 mW. Consistently, the observed payload of SMALLBug is relatively high, and sufficient to carry onboard power and control for future endeavors toward autonomy.

IV. LOCOMOTION EXPERIMENTS

We tested the locomotion capabilities of SMALLBug on a gridded foam display board by measuring its velocity when driven with actuation frequencies of 2, 10 and 20 Hz over a distance of 11 cm, while traveling along an approximately straight line in open loop. As seen in Fig. 8, the robot was recorded from a top view in order to measure the number of squares traveled; these three experiments are shown in the accompanying supplementary movie. The videos corresponding to the photographic sequences in Figs. 8(a)–(c), taken at 30 *frames per second* (fps), were analyzed using MATLAB's image processing toolbox to estimate the robot's position and velocity as functions of time; the resulting experimental positions over time are shown in Figs. 8(d)–(f). The estimated average speeds corresponding to the three actuation frequencies are shown in Table I. In this range, the relationship between the frequency of actuation and average speed is approximately linear with a slope of $0.81\,\mathrm{mm}\cdot\mathrm{s}^{-2}$.

As seen in the supplementary movie, each actuation frequency generates a distinct gait. At the *low* frequency of 2 Hz, SMALLBug moves according to a stepping pattern that we refer to as *crawling*. This locomotion mode resembles the gaits of inchworms and worm-inspired soft-robots such as those presented in [27]–[29]. At this actuation frequency, the robot achieves an average velocity of approximately $2.5\,\mathrm{mm}\cdot\mathrm{s}^{-1}$. At the moderate frequency of 10 Hz, the structure of SMALLBug oscillates quickly and smoothly, generating a locomotion mode that we refer to as *shuffling*. Accordingly, the resulting instantaneous velocity is approximately constant and does not experience sudden changes. At this actuation frequency, the robot achieves an average velocity of approximately $7\,\mathrm{mm}\cdot\mathrm{s}^{-1}$. Lastly, at the *high* actuation frequency of 20 Hz, SMALLBug generates small and fast periodic jumps that propel its body forward according to a locomotion mode that we refer to as *galloping*. We speculate that in this case, locomotion is produced by a periodic train of directional force-pulses acting on the very light mass (30 mg) of the robot; consistently, sudden changes in the locomotion speed can be observed. Also, in the particular case corresponding to the photographic sequence in Fig. 8(c), the velocity decreases during the last 2 s of the test. This deceleration might reflect the fact that after traveling a

TABLE I
VELOCITIES ACHIEVED BY SMALLBUG DURING LOCOMOTION EXPERIMENTS AT DIFFERENT ACTUATION FREQUENCIES

Frequency (Hz)	**Velocity** ($\text{mm}\cdot\text{s}^{-1}$)	**Gait**
2	2.5	Crawling
10	7	Shuffling
20	17	Galloping

relatively long distance (>10 cm), the tension produced by the Cu power wires prevents the SMALLBug prototype from moving freely. At this actuation frequency, the robot achieves an average velocity of approximately $17\,\text{mm}\cdot\text{s}^{-1}$.

V. CONCLUSIONS

We presented SMALLBug, a crawling microrobot that weighs only 30 mg, has a length of 13 mm and is driven by a 6-mg high-frequency flexible bending SMA actuator. The design, fabrication and functionality of the robotic components were thoroughly discussed, and the locomotion capabilities of SMALLBug were demonstrated through a series of experiments. Three actuator prototypes with thicknesses of 90, 180 and 230 µm were tested and characterized through experiments in which PWM inputs with a variety of DCs were used to find the empirical signal parameters that maximize the average MADOs. Using the collected information, we selected a 90-µm-thick actuator to drive SMALLBug. The resulting robotic prototype can be actuated at any frequency up to 20 Hz. We showed that depending on the frequency of actuation, SMALLBug can locomote according to three distinct gaits: crawling at 2 Hz, shuffling at 10 Hz and galloping at 20 Hz. Galloping produced the highest average locomotion speed, approximately $17\,\text{mm}\cdot\text{s}^{-1}$, which is equivalent to 1.3 BLPS. This speed is very high compared to those achieved by other state-of-the-art SMA-driven microrobots [10]–[13], especially considering the low mass of SMALLBug. A major contribution of the research presented in this letter is the empirical demonstration that high frequencies can be achieved using SMA-based actuation. Furthermore, we showed that this technology is suitable for the development of mobile microrobots as it enables the exploitation of the high work densities of SMA wires without sacrificing the speed of actuation.

REFERENCES

[1] Y. Wu, J. K. Yim, J. Liang, Z. Shao, M. Qi, J. Zhong, Z. Luo, X. Yan, M. Zhang, X. Wang, R. S. Fearing, R. J. Full, and L. Lin, "Insect-scale fast moving and ultrarobust soft robot," *Sci. Robot.*, vol. 4, no. 32, Jul. 2019, art. no. eaax1594.

[2] D. Lee, S. Kim, Y.-L. Park, and R. J. Wood, "Design of Centimeter-scale Inchworm Robots with Bidirectional Claws," in *Proc. 2011 IEEE Int. Conf. Robot. Automat. (ICRA)*, Shanghai, China, May 2011, pp. 3197–3204.

[3] B. Goldberg, R. Zufferey, N. Doshi, E. F. Helbling, G. Whittredge, M. Kovac, and R. J. Wood, "Power and Control Autonomy for High-Speed Locomotion With an Insect-Scale Legged Robot," *IEEE Robot. Automat. Lett.*, vol. 3, no. 2, pp. 987–993, Apr. 2018.

[4] D. S. Contreras, D. S. Drew, and K.S.J. Pister, "First Steps of a Millimeter-Scale Walking Silicon Robot," in *Proc. 2017 19th Int. Conf. Solid-State Sens., Actuators and Microsystems (Transducers)*, Kaohsiung, Taiwan, Jun. 2017, pp. 910–913.

[5] S. Hollar, A. Flynn, C. Bellew, and K.S.J. Pister, "Solar Powered 10 mg Silicon Robot," in *Proc. IEEE 16th Annu. Int. Conf. Micro Electro Mech. Syst. (MEMS)*, Kyoto, Japan, Jan. 2003, pp. 706–711.

[6] R. St. Pierre, W. Gosrich, and S. Bergbreiter, "A 3D-Printed 1 mg Legged Microrobot Running at 15 Body Lengths per Second," in *Solid-State Sens., Actuators, and Microsystems Workshop*, Hilton Head Island, SC, USA, Jun. 2018, pp. 59–62.

[7] W. Hu, G. Z. Lum, M. Mastrangeli, and M. Sitti, "Small-Scale Soft-Bodied Robot with Multimodal Locomotion," *Nature*, vol. 554, no. 7690, pp. 81–85, Jan. 2018.

[8] D. Vogtmann, R. St. Pierre, and S. Bergbreiter, "A 25 mg Magnetically Actuated Microrobot Walking at >5 Body Lengths/Sec," in *Proc. 2017 IEEE 30th Int. Conf. Micro Electro Mech. Syst. (MEMS)*, Las Vegas, NV, USA, Jan. 2017, pp. 179–182.

[9] H. Lu, M. Zhang, Y. Yang, Q. Huang, T. Fukuda, Z. Wang, and Y. Shen, "A Bioinspired Multilegged Soft Millirobot That Functions in Both Dry and Wet Conditions," *Nature commun.*, vol. 9, Sep. 2018, art. no. 3944.

[10] K. Saito, K. Iwata, Y. Ishihara, K. Sugita, M. Takato, and F. Uchikoba, "Miniaturized Rotary Actuators Using Shape Memory Alloy for Insect-Type MEMS Microrobot," *Micromachines*, vol. 7, no. 4, Apr. 2016, art. no. 58.

[11] A. Menciassi, D. Accoto, S. Gorini, and P. Dario, "Development of a Biomimetic Miniature Robotic Crawler," *Auton. Robots*, vol. 21, no. 2, pp. 155–163, Jan. 2006.

[12] A. M. Hoover, E. Steltz, and R. S. Fearing, "RoACH: An Autonomous 2.4g Crawling Hexapod Robot," in *Proc. 2008 IEEE/RSJ Int. Conf. Intell. Robots and Syst. (IROS)*, Nice, France, Sep. 2008, pp. 26–33.

[13] B. Kim, M. G. Lee, Y. P. Lee, Y. Kim, and G. Lee, "An Earthworm-Like Micro Robot Using Shape Memory Alloy Actuator," *Sens. and Actuators A: Physical*, vol. 125, no. 2, pp. 429–437, Jan. 2006.

[14] D. C. Lagoudas (Editor), *Shape Memory Alloys: Modeling and Engineering Applications*. New York, NY, USA: Springer, 2008.

[15] S. Lederlé, "Issues in the Design of Shape Memory Alloy Actuators," Master's thesis, Massachusetts Institute of Technology (MIT), Jun. 2002.

[16] K. Otsuka and C. M. Wayman (Editors), *Shape Memory Materials*. Cambridge, UK: Cambridge University Press, 1999.

[17] J. Z. Ge, L. Chang, and N. O. Pérez-Arancibia, "Position Control of a Shape-Memory Alloy Actuator Using a Preisach-Model-Based Inverse-Temperature Method," in *Proc. 2019 American Control Conf. (ACC)*, Philadelphia, PA, USA, Jul. 2019, pp. 3801–3808.

[18] S.-H. Song, H. Lee, J.-G. Lee, J.-Y. Lee, M. Cho, and S.-H. Ahn, "Design and Analysis of a Smart Soft Composite Structure for Various Modes of Actuation," *Composites Part B: Eng.*, vol. 95, pp. 155–165, Jun. 2016.

[19] S.-H. Song, J.-Y. Lee, H. Rodrigue, I.-S. Choi, Y. J. Kang, and S.-H. Ahn, "35 Hz Shape Memory Alloy Actuator with Bending-Twisting Mode," *Scientific Rep.*, vol. 6, Feb. 2016, art. no. 21118.

[20] R. J. Wood, S. Avadhanula, R. Sahai, E. Steltz, and R. S. Fearing, "Microrobot Design Using Fiber Reinforced Composites," *J. Mech. Des.*, vol. 130, no. 5, May 2008, art. no. 052304.

[21] S. Maeda, Y. Hara, T. Sakai, R. Yoshida, and S. Hashimoto, "Self-Walking Gel," *Adv. Mater.*, vol. 19, no. 21, pp. 3480–3484, Nov. 2007.

[22] M. Duduta, D. R. Clarke, and R. J. Wood, "A High Speed Soft Robot Based on Dielectric Elastomer Actuators," in *Proc. 2017 IEEE Int. Conf. Robot. Automat. (ICRA)*, Singapore, May–Jun. 2017, pp. 4346–4351.

[23] X. Ji, X. Liu, V. Cacucciolo, M. Imboden, Y. Civet, A. El Haitami, S. Cantin, Y. Perriard, and H. Shea, "An Autonomous Untethered Fast Soft Robotic Insect Driven by Low-Voltage Dielectric Elastomer Actuators," *Sci. Robot.*, vol. 4, no. 37, Dec. 2019, art. no. eaaz6451.

[24] B. Shin, J. Ha, M. Lee, K. Park, G. H. Park, T. H. Choi, K-J. Cho, and H-Y. Kim, "Hygrobot: A Self-Locomotive Ratcheted Actuator Powered by Environmental Humidity," *Sci. Robot.*, vol. 3, no. 14, Jan. 2018, art. no. eaar2629.

[25] Y. Ma, Y. Zhang, B. Wu, W. Sun, Z. Li, and J. Sun, "Polyelectrolyte Multilayer Films for Building Energetic Walking Devices," *Angewandte Chemie Int. Ed.*, vol. 50, no. 28, pp. 6254–6257, Jul. 2011.

[26] D. Morales, E. Palleau, M. D. Dickey, and O. D. Velev, "Electro-Actuated Hydrogel Walkers With Dual Responsive Legs," *Soft Matter*, vol. 10, no. 9, pp. 1337–1348, Mar. 2014.

[27] A. A. Calderón, J. C. Ugalde, L. Chang, J. C. Zagal, and N. O. Pérez-Arancibia, "An Earthworm-Inspired Soft Robot with Perceptive Artificial Skin," *Bioinspir. Biomim.*, vol. 14, no. 5, Sep. 2019, art. no. 056012.

[28] J. Z. Ge, A. A. Calderón, L. Chang, and N. O. Pérez-Arancibia, "An Earthworm-Inspired Friction-Controlled Soft Robot Capable of Bidirectional Locomotion," *Bioinspir. Biomim.*, vol. 14, no. 3, May 2019, art. no. 036004.

[29] K. Xu and N. O. Pérez-Arancibia, "Electronics-Free Logic Circuits for Localized Feedback Control of Multi-Actuator Soft Robots," *IEEE Robot. Automat. Lett.*, vol. 5, no. 3, pp. 3990–3997, Jul. 2020.

[30] J. N. Reddy, *Mechanics of Laminated Composite Plates and Shells: Theory and Analysis*. Boca Raton, FL, USA: CRC Press, 2003.